Structural Insights into the Activation of ATM Kinase

Jianxiong Xiao[1,2#], Mengjie Liu[1,2#], Yilun Qi[1#], Yuriy Chaban[3#], Chao Gao[1#], Beiqing Pan[1], Yuan Tian[1], Zishuo Yu[1], Jie Li[4], Peijun Zhang[3,5], and Yanhui Xu[1,2,6,7 *]

[1]Fudan University Shanghai Cancer Center, Institutes of Biomedical Sciences, State Key Laboratory of Genetic Engineering and Key Laboratory of Medical Epigenetics and Metabolism, Shanghai Medical College of Fudan University, Shanghai 200032, China.

[2]Key Laboratory of Molecular Medicine, Ministry of Education, Department of Systems Biology for Medicine, School of Basic Medical Sciences, Shanghai Medical College of Fudan University, Shanghai 200032, China.

[3]Electron Bio-Imaging Centre, Diamond Light Sources, Harwell Science and Innovation Campus, Didcot, Oxfordshire, United Kingdom

[4]National Facility for Protein Science in Shanghai, Zhangjiang Lab, Shanghai, 201210, China

[5]Division of Structural Biology, Wellcome Trust Centre for Human Genetics, University of Oxford, Oxford, United Kingdom.

[6]Collaborative Innovation Center of Genetics and Development, School of Life Sciences, Fudan University, Shanghai 200433, China.

[7]CAS Center for Excellence in Molecular Cell Science, Chinese Academy of Sciences, Shanghai, 200031, China.

[#] These authors contributed equally to this work.

[*] To whom correspondence should be addressed. E-mail: xuyh@fudan.edu.cn

Running title: Cryo-EM structures of monomeric and dimeric ATM

Key words: ATM, Activation, PIKK kinases, Structure, Cryo-Electron Microscopy

Abstract

ATM is a giant protein kinase that responses DNA damages and activates cell cycle checkpoint, transcription, DNA repair, and apoptosis pathways. The activation of ATM kinase activity is essential for DNA damage response but the mechanism remains controversial. We found that ATM prefers dimeric form whereas monomer is enzymatically more active. We determined the cryo-EM structures of human ATM dimer at 4.3 Å and monomer at 7.8 Å resolution, respectively. In ATM dimer, the PRD domain is stabilized by TRD3 of the other ATM molecule and adopts a restrained conformation to prohibit substrate entry and inhibit kinase activity. In ATM monomer, the PRD tends to be more flexible and allow the kinase domain to be more open and adopt an active conformation. Dimer-to-monomer transition and DNA association independently activate ATM through releasing otherwise inhibitory conformation of the dimer. Our study reveals the mechanism for activation of ATM.

Introduction

ATM (ataxia telangiectasia-mutated) is a master regulator in response to DNA damage and activates downstream pathways including cell cycle checkpoints, DNA damage repair, transcription, immunity, the central nervous system development and metabolism[1,2]. Loss of ATM activity in human results in the pleiotropic neurodegeneration disorder ataxia-telangiectasia(A-T) that is characterized by immunodeficiency, cancer predisposition, premature aging and insulin-resistant diabetes[3,4].

ATM is a giant protein kinase that belongs to the family of phosphoinositide-3-kinase-related kinases (PIKKs). ATM, and two other PIKK family members, ATM- and Rad3-related (ATR), DNA-dependent protein kinase catalytic subunit (DNA-PKcs), are key cellular regulators in response to DNA damage. Like other PIKK family members, ATM has a large N-terminal α-solenoid, a FAT (FRAP, ATM, TRRAP) domain, a conserved kinase domain (KD) followed by a C-terminal short segment (FATC) [5,6].

ATM is activated in response to DNA damage and activates cell cycle checkpoint, transcription, DNA repair, and apoptosis pathways through phosphorylating a large number of substrates including Chk2 and p53[4,7,8]. Thousands of proteins have been identified as potential ATM substrates[9,10]. The activation of ATM kinase activity is a key process to properly transmit the DNA damage signals to the downstream pathways[3,7]. The mechanism for ATM activation has been extensively studied and distinct models were proposed.

DNA damages induce ATM activation accompanying a dimer-to-monomer transition and autophosphorylation of residue S1981[11]. MRN (Mre11-Rad50-Nbs1) complex senses the DNA damages and stimulate the kinase activity of ATM[12,13] and DNA ends are also involved in the ATM activation[14,15]. Thus, dimer-to-monomer transition has been proposed to be a key process for ATM activation[11-15]. However, the existence of ATM monomer and the causal correlation between

monomerization and activation have never been confirmed in biochemical analysis using purified proteins or in structural analyses.

The majority of previous structural studies showed that ATM adopts dimeric form[16-18] although some negative stain EM studies suggested the existence of ATM monomer[18,19]. A recent study proposed that ATM undergoes conformational changes between an inactive closed dimer and an active open dimer[17]. Despite extensive studies over the past two decades, it remains controversial how ATM is activated. Particularly, whether ATM exists in a monomeric form, whether the monomer is more active than dimer, and how dimer-to-monomer transition affects the ATM kinase activity, remain elusive.

Here we report the cryo-EM structures of human ATM dimer at 4.3 Å resolution and monomer at 7.8 Å resolution, respectively. The EM map of the core kinase domain of ATM dimer was locally refined to 4.0 Å resolution. We found that ATM monomer is catalytically more active than ATM dimer and that dimer-to-monomer transition and DNA association independently activate ATM through releasing otherwise inhibitory conformation of the PRD (PIKK regulatory domain) in dimer. The structural and biochemical analyses together provide a structural model for understanding the mechanisms of ATM activity regulation. Our study also provides a framework for understanding the regulation of ATM-mediated DNA damage response.

Results

ATM monomer is catalytically more active than ATM dimer

To prepare ATM proteins for biochemical and structural studies, we overexpressed human ATM in HEK 293 suspension cells. We tested various purification approaches to investigate whether ATM exists in a monomeric form *in vitro*. In most cases, the purified ATM existed in a dimeric form, as determined by glycerol gradient centrifugation and negative stain EM analyses. Monomeric ATM could be obtained when the cells were lysed using homogenizer in a buffer lacking DNase I (Fig. 1).

To separate the ATM monomer from large amount of dimer, we performed glycerol gradient centrifugation, in which two peaks were fairly separated (Fig. 1a). The oligomerization states of corresponding peak fractions were detected using negative-stain EM and two-dimensional (2D) class averages, which clearly revealed well-separated monomeric and dimeric ATM (Fig. 1b, 1c). The above results confirm the existence of monomeric and dimeric ATM. The two peak fractions were used in the following biochemical and structural analyses.

The generation of monomeric ATM is probably induced by double strand breaks (DSBs) during cell disruption in the absence of DNase I. This approach is essentially similar to previously described method[14]. Notably, the ATM dimer is fairly stable and unable to dissociate into monomer even in very low concentration whereas the freshly purified ATM monomer tends to gradually dimerize in protein concentration higher than 0.22 mg/ml (data not shown). The sample scarcity and dimerization tendency might hamper the preparation of ATM monomer in previous studies.

To compare the kinase activities of dimeric and monomeric ATM, we performed an *in vitro* kinase assay using two representative substrates, the purified human p53 and Chk2 (kinase dead mutant, referred to as Chk2 below)[20]. The monomeric ATM shows kinase activity ~10-fold higher

than the dimeric ATM (Fig. 1d, Supplementary Fig. 1a). No obvious difference in the level of S1981 autophosphorylation was observed between the two ATM forms (Supplementary Fig. 1b), in agreement with previous studies[15]. The dimeric ATM could be activated by the addition of H_2O_2, indicating a functional dimer used in the assay[21] (Supplementary Fig. 1c). Therefore, ATM monomer is enzymatically more active than dimer and such difference is independent of ATM autophosphorylation at S1981.

Structure determination of ATM dimer and monomer

We next determined the cryo-EM structures of dimeric and monomeric ATM using single particle reconstructions (Supplementary Figs. 2-3, movies S1-S2). The cryo-EM maps of ATM dimer and monomer were refined to 4.3 and 7.8 Å resolution, respectively. The EM maps of the C-terminal core region and the N-terminal α-solenoid of dimer were locally refined to 4.0 Å and 5.8 Å resolution, respectively. The structural model of ATM dimer was built by fitting previously reported dimeric ATM structure[17] into the EM density and manually model building. The model of ATM monomer was built by flexible fitting and manually building using the dimer structural model as template (Supplementary Table 1).

Structure of ATM dimer

The ATM dimer adopts a similar fold to that of previously reported ATM dimer in the closed form[17]. Notably, the open form ATM dimer was not observed in our study. The structure reveals a butterfly architecture with two monomers arranged in a two-fold symmetry (Fig. 2b, 2d, Fig.3a). Like other PIKK members, ATM possesses a large N-terminal α-solenoid, followed by a FAT (FRAP, ATM, TRRAP) domain, a conserved kinase domain (KD), and a C-terminal short segment (FATC)[5,6] (Fig. 2a). Each monomer has an N-terminal superhelical α-solenoid (designated N^{ATM}),

followed by a C-terminal compact core containing the FAT, KD, and FATC domains (designated C^{ATM}) (Fig. 2a, 2c, Fig. 3e). The N^{ATM} consists of a 1.3-turn left-handed α-solenoid (N1) followed by an extended HEAT repeats (N2) and a disconnected helix-bundle (N3) (Fig. 2c, Fig. 3d). The $N3^{ATM}$ bridges $N2^{ATM}$ and the C^{ATM}. The FAT domain contains three tetratricopeptide repeat domains (TRD), TRD1 (fα1 to fα4, f represents FAT), TRD2 (fα5 to fα13), and TRD3 (fα14 to fα23), followed by a short HEAT-repeats domain (HRD) (fα24 to fα29). The FAT domain adopts a C-shaped conformation and wraps around the KD (Fig. 2e, Fig. 3e, 3f).

The ATM dimerization is mediated by the two C^{ATM} (Fig. 2d, 2f, 2g). In the lower interface, three continuous helices (fα5 to fα7, residues 2041-2085) of TRD2 and helix fα16 (residues 2268-2281) of TRD3 pack against the four equivalent helices of ATM' (' represents the other ATM molecule) (Fig. 2g). In the upper interface, a four-helix bundle (fα19 to fα22) of the TRD3 makes extensive contacts with the C-lobe of ATM' (Fig. 2d, 2f). The two parallel helices kα10/10' (k represents kinase domain) are sandwiched by helices fα21-22/fα21'-22'. A loop connecting fα19 and fα20 packs against the FATC' of the KD'. The helices fα21-fα22 of TRD3 and kα9a' and kα10' of the KD' and together buttress the kinase domain. The protruded portion of the two long α helices (fα21-fα22) (designated TRD3 dimeric helices, TRD3-DH) packs against two kinase regulatory elements of the other ATM molecule: the kα9b'-9c' and the activation loop of the KD' (Fig. 2d). The PIKK regulatory domain (PRD) consisting kα9b-9c and the following linker is predicted to prohibit substrate entry and inhibit kinase activity in PIKK kinases[22]. In ATM dimer, the PRD' is well-ordered because of stabilization by the TRD3-DH and helices kα9a' and kα10' of the KD', supporting an inhibitory function.

The monomer structure reveals a more open catalytic pocket

The structure of ATM monomer reveals a similar overall fold to one copy of ATM in the dimeric form (Fig. 3b, 3c, Fig. 4a). Compared to ATM dimer, the monomer reveals a more open catalytic pocket due to lack of stabilization by dimer contacts (Fig. 4, movie S3). In particular, the height of catalytic pocket, as represented by the distance between LBE (LST8 binding element) and HRD, is 43.3 Å in dimer and 47.1 Å in monomer. The width of the catalytic pocket, as represented by the distance between kα1 and helices kα10, is 52.6 Å in dimer and 59.7 Å in monomer (Fig. 4a). Thus, the associated PRD tends to be more flexible due to less restraint by kα9a and kα10 and lack of stabilization by otherwise associated TRD3-DH' in ATM dimer. The EM density indicates that the PRD is highly dynamic and disordered in ATM monomer, indicating a less restrained catalytic pocket that is more favorable for substrate entry. The conformational switch of PRD is probably the key for the activation of ATM kinase (Fig. 4, movie S4). Thus, ATM adopts an autoinhibitory conformation in dimeric form and monomerization releases such inhibition and enhances the kinase activity.

The pattern of ATM dimerization is generally similar to ATR-ATRIP complex[23], but distinct from other PIKK complexes[24-28] (Supplementary Fig. 4). However, ATR dimer-to-monomer transition has never been reported, probably because ATR dimerization is mediated by both upper and lower interfaces of C^{ATR} dimer contacts[23]. In contrast, the ATM dimer has less contacts at the lower dimer interface and dimerization is primarily mediated by the upper interface, which might serve as a targeting site for regulation (Supplementary Fig. 5). If this upper interface is disrupted by some regulatory factors, the dimer would not be maintained and active monomers are formed.

To test the effect of PRD and TRD3-DH on the dimer-to-monomer transition and the regulation of kinase activity, we made four internal deletions of ATM: $ATM^{\Delta PRD}$ (Δ2964-2998), $ATM^{\Delta PRD\text{-}S}$ (Δ2981-2998, the invisible linker, S represents short), $ATM^{\Delta DH}$ (Δ2408-2450, TRD3-DH), and $ATM^{\Delta DH\text{-}S}$ (Δ2422-2435, the invisible linker). The four mutants were purified using

glycerol gradient centrifugation and the fractions at dimer position were used in the *in vitro* kinase activity assay. Interestingly, all the four ATM mutants tend to form monomer in solution compared to the wild type ATM (Fig. 4c, Supplementary Fig. 6), indicating that PRD and TRD3-DH involve ATM dimerization. As predicted, $ATM^{\Delta PRD}$ and $ATM^{\Delta PRD\text{-}S}$ showed robust activation of kinase activities compared to the wild type ATM, supporting the key role of PRD in inhibiting the kinase activity. Unexpectedly, $ATM^{\Delta DH}$ and $ATM^{\Delta DH\text{-}S}$ showed similar (p53 as substrate) or even decreased (Chk2 as substrate) kinase activities compared to the wild type ATM (Fig. 4d). The deletion of TRD3-DH may not be sufficient to release the inhibition by PRD, which is still supported by helices kα9a and kα10. Alternatively, the TRD3-DH might be also required for phosphorylation of substrates like Chk2.

DNA fragments directly stimulate ATM kinase activity

Biochemical studies have shown that ATM can be activated by MRN complex and DNA fragments[12,14,15,29]. To further investigate the mechanism of ATM activation, we performed an *in vitro* ATM kinase assay using purified MRN complex and DNA fragments (Fig. 5). The kinase activity of ATM dimer could be stimulated by MRN complex in a low salt (50 mM KCl) condition but not in higher salt (200 mM KCl) condition, suggesting that ATM-MRN association is not well-maintained in high salt condition. In contrast, ATM dimer kinase activity was largely enhanced by the addition of double strand (ds)DNA even in the high salt condition. Moreover, the level of S1981 autophosphorylation was stimulated by dsDNA (Supplementary Fig. 7b). The presence of MRN did not further enhance ATM activity, indicating that DNA is sufficient to stimulate ATM kinase activity.

We next investigated the mechanism of DNA-mediated activation of ATM. The kinase activity of dimeric ATM was enhanced by the addition of increasing amount of dsDNA (Fig. 6a,

6b). The concentration of free DNA ends is the key for the activation. Similar concentration of DNA fragments with various lengths (360bp, 950bp, and 1800bp) showed comparable activity enhancement, suggesting the length of DNA is not a key factor for the activation. In addition, the linearized DNA is better than circular plasmid in activating ATM (Supplementary Fig. 7c). The linearized DNA with blunt ends is better than that with single-stranded overhangs. This suggests that the activation of ATM by dsDNA is primarily dependent on the concentration and type of free DNA ends.

Previous studies indicated that only the dsDNA longer than 200bp could efficiently activate ATM[14,30]. Surprisingly, we detected obvious ATM activation by a 30bp dsDNA and a 30nt single stranded (ss)DNA although the ssDNA showed relatively weak stimulation (Fig. 6c, Supplementary Fig. 7d). A 54bp dsDNA showed more robust stimulation of ATM activity than 30bp dsDNA did. The ATM activity could be effectively stimulated by 1.8kb dsDNA even in a concentration 100-fold lower than 30bp or 54bp DNA. This observation suggests that DNA-mediated ATM activation is dependent of DNA length with a certain range (shorter than ~54bp) but independent of DNA length when DNA is longer than several hundred base pairs (Fig. 6a, 6b).

Although ATM monomer is enzymatically more active than ATM dimer (Fig. 1d), ATM monomer activity can be further stimulated by DNA fragments (Fig. 6d), indicating that DNA stimulates ATM activity independent of oligomerization state. The four ATM mutants, $ATM^{\Delta PRD}$, $ATM^{\Delta PRD\text{-}S}$, $ATM^{\Delta DH}$, and $ATM^{\Delta DH\text{-}S}$ could not be stimulated by dsDNA (Fig. 6e), suggesting that these regulatory elements (PRD and TRD3-DH) are required for DNA-mediated activation. Consistently, oxidative crosslinking of C2291/C2291' may lead to close association of two PRD domains and release autoinhibition in the context of ATM dimer[21]. Therefore, the above observations indicate a combinatorial mechanism for activation of ATM, the dimer-to-monomer transition and DNA-mediated activation.

We here proposed a model for ATM activation in response to DNA damage (Fig. 6f). The ATM dimer adopts an autoinhibitory fold, in which the PRD is restrained in an inhibitory conformation by kα9a, kα10 and TRD3-DH'. The well-positioned PRD prohibits substrate entry and inhibits kinase activity of ATM. Upon the formation of monomeric ATM, the PRD is more flexible because of lacking stabilization by TRD3-DH and less support by kα9a and kα10. The ATM monomer can be further activated by dsDNA in a manner dependent of the concentration and type of free DNA ends. These regulatory elements (PRD and TRD3-DH) are also required for DNA-mediated activation of ATM, suggesting that DNA may also regulate the conformation of PRD and TRD3-DH for activation. Thus, dimer-to-monomer transition and DNA association independently release the inhibitory conformation of PRD and collectively lead to a fully-activated ATM for substrate phosphorylation. MRN and other factors may facilitate the recruitment of ATM to the broken DNA ends upon DNA damage.

Discussion

The activation of ATM is key for the regulation of DNA damage response pathway and has been extensively studied in the past two decades[7,8,31]. Previous cryo-EM studies show ATM dimer forms an open dimer and a tightly packed closed dimer and proposed that the conformational switch regulates the kinase activity of ATM[17], challenging the activation model derived from previous biochemical studies. There are also different models about DNA-mediated activation of ATM[11,12,15]. The lack of well-defined kinase assay system prevents solving the puzzles.

In this work, we successfully isolated ATM monomer and dimer to homogeneity and set up *in vitro* kinase assay using purified p53 and Chk2 as substrates. Taking advantage of the well-defined biochemical assays, we demonstrated that ATM monomer is more active than ATM dimer in terms of kinase activity in a manner independent of the S1981 autophosphorylation. Cryo-EM structures of ATM monomer and dimer show distinct features of the catalytic pocket and reveal the mechanism for the activation of ATM upon dimer-to-monomer transition. Following up biochemical analyses indicated that ATM activation by monomerization and DNA association both depend on the conformational regulation of the PRD domain. Thus, our work addressed long-standing questions in the studies of activation of ATM.

We suspect that dimer-to-monomer transition is induced by DSBs during the cell homogenization because the ATM monomer could not be obtained when the cells are disrupted in the presence of DNase I. In the *in vitro* assays, ATM kinase activity was stimulated by DNA ends in a manner independent of MRN complex. DNA stimulates ATM kinase activity but does not directly promotes dimer-to-monomer transition (data not shown). These observations suggest that the DSBs and other factors together promote dimer-to-monomer transition, likely after the recruitment of ATM dimer to the broken DNA ends. Thus, the DNase I-mediated fragmentation of genomic DNA may disrupt DSB-associated complexes and prevent ATM monomerization.

ATM dimer is fairly stable and does not dissociate into monomer in low protein concentration (~ 0.02 mg/ml) or under conditions of high salt concentration (~500 mM KCl). In contrast, the purified monomer is unstable and tends to dimerize when the protein concentration is higher than 0.22 mg/ml. Therefore, ATM monomer represents a transient state in response to DNA damages and turns back into dimeric form under precise regulation to avoid persistent activation. Consistently, the maintenance of ATM in active monomer requires ATM binding factors like NBS1 or ATMIN[32,33].

ATM kinase activity is regulated through two critical elements, the PRD and TRD-DH domains. The characteristic TRD-DH region of ATM is longer than that of other PIKK members (Supplementary Fig. 4). The deletion of TRD-DH impairs DNA-mediated ATM activation, supporting an essential role of TRD-DH in activation of ATM. In contrast, the deletion of PRD enormously stimulates kinase activity of ATM. Similar role PRD in regulation of kinase activity has been demonstrated in other PIKK members including mTOR, ATR, and DNA-PKcs [22-24,34]. Moreover, H_2O_2 activates ATM dimer through promoting a disulfide bond formation between residues C2991 (within the PRD) and C2991'[21]. Thus, TRD-DH and PRD play distinct roles and coordinately regulates the conformation of catalytic cavity of ATM.

Structural comparison of ATM dimer and monomer indicates that other regions, such as kα10 and FACT domain that are close to the dimer interface and HRD that supports the catalytic pocket, also undergo significant conformational changes upon transition from dimer to monomer (Fig. 4). Interestingly, these regions also involve regulation of ATM kinase activity. For example, Notch and FOXO3a competitively bind to part of kα10 and FACT domain and regulate the kinase activity of ATM[31,35,36]. Residues R2579 and R2580 within the HRD domain are essential for ATM activation by MRN and DNA[37]. Thus, ATM kinase activity is regulated through changing the conformation of the kinase domain by distinct mechanisms in response to various upstream signals.

Materials and Methods

Reagents

Antibodies against phosphor-Thr68 of Chk2 (Cat# 2661) and phosphor-Ser15 of p53 (Cat# 9284) were purchased from Cell Signaling Technology; Antibodies against phosphor- Ser1981 of ATM (Cat# AP0310) was from ABclonal; horseradish peroxidase-labeled anti-rabbit secondary antibody was from AbMart; anti-Flag M2 affinity agarose gel was from Sigma; GST resin and Mono S were from GE Healthcare; polyethyleneimine (PEI) was from Polysciences (23966).

Protein expression and purification

Codon-optimized full-length ATM ORF (open reading frame) was sub-cloned into a modified pCAG vector, which contains N-terminal FLAG tag, protein A (ProA) tag, and 3C protease cutting site followed by MCS (multiple cloning sites). The plasmid was transfected into Expi293F cells using PEI followed by further culture at 37 °C for 3 days. Protein purification was carried out as described previously with minor modifications[14,18]. Cells were harvested and lysed by homogenization on ice in lysis buffer containing 50 mM HEPES (pH 7.4), 400mM KCl, 20 mM NaCl, 20% (v/v) glycerol, 10 mM $MgCl_2$, 0.5 mM phenylmethylsulphonyl fluoride (PMSF), 1 mM Tris(2-carboxyethyl) phosphine hydrochloride (TCEP), 5 mM ATP, 10 Mm NaF, 1 μg/ml pepstatin, 1μg/ml leupeptin, and 1μg/ml aprotinin. After centrifugation at 15000 rpm for 30 min at 4°C, supernatants were incubated with anti-Flag M2 affinity agarose gel for 2 h at 4°C. The resins were thoroughly washed with the lysis buffer. The fusion proteins were digested using 3C protease overnight and the free ATM proteins were eluted with a buffer containing 25 mM HEPES (pH 7.4), 400 mM KCl, 15% (v/v) glycerol, 10 mM $MgCl_2$, and 1 mM TCEP. The eluted proteins were further purified using a cation exchange column (Mono S). The peak fractions were collected

for kinase assay and following purification. The four ATM mutants were overexpressed and purified using similar procedures.

To prepare the MRN complex, the ORFs of Mre11, Rad50, and Nbs1 were sub-cloned into a modified pCAG vector containing N-terminal protein A (ProA) tag, respectively. The three plasmids were co-transfected to Expi293 cells using PEI and the cells were further cultured at 37 °C for 3days. The cells were harvested and lysed in a lysis buffer containing 50 mM Tris-HCl (pH 7.4), 300 mM NaCl, 0.3% (v/v) Tween, 5 mM ATP, 5 mM $MgCl_2$, 1 mM TCEP, 10% (v/v) Glycerol, 0.5 mM PMSF, 1 μg/ml Aprotinin, 1 μg/ml Pepstatin, 1 μg/ml Leupeptin at 4°C for 30 min. The lysate was clarified by centrifugation at 15,000 rpm at 4°C for 40 min and the supernatant was incubated with IgG resin for 3 h and the resins were thoroughly washed with the lysis buffer. The fusion proteins were digested using 3C protease at 4°C overnight to remove tags and eluted with a buffer containing 50 mM Tris-HCl (pH 7.4), 300 mM NaCl, 0.3% (v/v) Tween, 1 mM TCEP, 10% (v/v) Glycerol. Then the complex was purified by mono Q column. The peak fractions were collected and stored at -80°C for *in vitro* kinase assays.

The ORF of kinase-dead Chk2 (K249R) was sub-cloned into a modified pGEX-6P-1 vector and overexpressed in E. coli BL21 (DE3) cells. The fusion protein was purified by GST affinity column and digested using 3C protease overnight to remove tags. The protein was directly eluted by an elution buffer containing 30 mM Tris-HCl (pH 8.0), 300 mM NaCl, 3mM DTT. The eluted protein was stored at -80 °C for *in vitro* kinase assays.

The full length p53 protein was prepared as previously described[24].

Glycerol gradient sedimentation

The glycerol gradient was generated using a light solution containing 10% (v/v) glycerol, 300 mM KCl, 30 mM HEPES, pH 7.4, 5 mM $MgCl_2$, 1 mM TCEP), and a heavy solution containing 30%

(v/v) glycerol, 300 mM KCl, 30 mM HEPES, pH 7.4, 5 mM $MgCl_2$, 1mM TCEP. Centrifugation was performed at 38,000 r.p.m. in a SW41Ti swinging bucket rotor for 18h at 4 °C. The fractions (200 µl each) were analyzed by SDS-PAGE and EM immediately. The peak fractions were exchanged into a buffer containing 300 mM KCl, 30 mM HEPES, pH 7.4, 5 mM $MgCl_2$, 1mM TCEP and concentrated for Cryo-EM grids preparation.

In vitro kinase activity assays

The kinase assays were adapted from published protocols for ATM[14,38] . In brief, 0.7 µg p53 or 1µg Chk2 (K249R) was incubated with ATM in 20 µl reaction buffer containing 50 mM HEPES, pH 7.4, 50 mM KCl, 5% glycerol, 5 mM $MgCl_2$, 2 mM ATP, and 1mM TCEP at 30 °C for 90 min. For the reactions with DNA or MRN complex, ATM was first incubated with DNA or MRN complex at 30º C for 30 min and then the substrate was added followed by further incubation at 30º C for 60 min. Reactions were terminated by the addition of SDS-PAGE sample loading buffer and analyzed by western blotting. Western blotting results were quantified by ImageJ program.

The long dsDNA fragments of different lengths were generated by PCR. The 360bp, 950bp, and 1.8kb PCR products were amplified from the plasmids containing ORFs of CTF8, ELP5, and ATM, respectively. All PCR products were gel-purified. The 30nt ssDNA (5'-CTGAATACTAGATGCG GTCCTCAAGCTGAT -3'), 30bp dsDNA (F strand 5'- CTGAATACTAGATGCGGTCCTCAA GCTGAT-3'; R strand 5'- ATCAGCTTGAGGACCGCATCTAGTATTCAG-3'), and 54bp dsDNA (F strand 5'-GGCCGCACGCGTCCACCATGGGGTACAACTACGATCTAGCTTCAT GCACCGGAC -3'; R strand 5'-GTCCGGTGCATGAAGCTAGATCGTAGTTGTACCCCATG GTGGACGCGTGCGGCC-3') were synthesized and annealed by mixing equimolar amounts of the F strand and R strand oligonucleotides at a final concentration of 100 µM in TE buffer. The

annealing was performed by heating to 95 °C for 10 min followed by slowly cool down to room temperature.

EM grids preparation

Negative staining was used to evaluate the protein quality. In brief, 5 µl of freshly purified ATM (~50 nM) was applied onto copper grids supported by a thin layer of glow-discharged carbon film (Zhongjingkeyi Technology Co., Ltd). After adsorption for 1 min, 2%(w/v) uranyl acetate was used for negative staining at room temperature. The negative stained grid was examined using FEI Talos L120C operated at 120 KeV.

Cryo-grid preparation was performed using FEI Vitrobot mark IV operated at 9 °C and 100% humidity. Aliquots of 4 µl of freshly purified ATM dimer (~ 0.6 mg/ml) /ATM monomer (~ 0.2 mg/ml) were applied to glow-discharged holey carbon grids (Quantifoil Au, R1.2/1.3, 300 mesh). The grids were blotted using filter paper and then flash-plunged into liquid ethane pre-cooled in liquid nitrogen.

EM data acquisition

Cryo-EM data were collected at 300 KeV acceleration voltage on Titan Krios microscope at electron Bio-Imaging Centre (eBIC), Diamond Light Source Ltd, UK [39]. All data were collected in movie mode [40]. ATM monomer data were collected using Falcon III detector in electron-counting mode at nominal magnification 120,000 resulting in pixel size 0.66 Å and total dose ~32 ē/Å^2, and collected using Volta Phase plate with underfocus set to 0.7 and 0.9 µm.

Movies of ATM dimer were collected using K2 direct electron detector mounted after Gatan energy filter with 20ēV slit at nominal magnification 165,000, resulting in pixel size 0.81 Å and total dose 38 e/ Å^2. EPU automated acquisition software was used for data collection. On-the-fly

data processing was performed using Scipion[41]. Movies were aligned and dose weighted using MotionCorr2.0[42]. CTF parameters were estimated using GCTF [43]. All subsequent data analysis was performed using Relion package [44].

Image processing of ATM dimer

4524 movies of ATM dimer were selected for analysis (Supplementary Figure 2b). Particles were initially picked using a Gaussian blob, and reference-free 2D classes were calculated in Relion. Best 2D classes were used as template for second iteration of particle picking. About 915,000 particles were extracted and analysed. Particles were coarsened for initial rounds of analysis 8 times to speed up data processing. Final coarsening was 2 times, resulting in pixel size 1.62 Å/pixel. After several rounds of 2D classification 287,832 particles from the best 2D classes were selected (Supplementary Figure 2c). They were subjected to 3D classification using 3D reference generated from PDB model 5np0 and using C2 symmetry. Despite our effort to remove bad particles, one 3D class with 1,099 particles represented collection of artefacts (not shown), while the other with 54,318 members almost entirely consisted of bottom views (Supplementary Figure 2a). These two classes were removed from further analysis. Remaining 3 classes were essentially the same, but had different (and mostly complementary) angular distribution profiles (Supplementary Figure 2a). These classes, containing 232,416 particles between them, were combined and subjected to 3D refinement with C2 symmetry. Obtained 3D map had average resolution 4.27 accordingly to corrected gold-standard FSC 0.143 criteria. (Supplementary Figure 2a, g). The resolution varied between 4-6 Å for C-terminal, and 6-8 Å for N-terminal domains (Supplementary Figure 2e, f). Focused refinement of C-terminal domain helped to improve its resolution to 4.03 Å. In order to improve the resolution of N-terminal domain, each monomer of the ATM dimer was subtracted and the data containing each

half of ATM dimer densities were combined. Resulting data set with double the number of signal subtracted particles were subjected to 3D refinement with C1 symmetry against re-centred model of a single ATM monomer extracted from the dimer model. Resulting 3D model had overall resolution 4.37 Å, with resolution of N-terminal domain has improved to 5.76 Å (Supplementary Figure 2a, g).

Image processing of ATM monomer

For ATM-monomer, MotionCor2s[42] was used to pre-process the movie stack through all frames. The contrast transfer function parameters were estimated by Gctf from non-dose-weighted micrographs and other procedures of data processing were performed within RELION 3.0 using the dose-weighted micrographs[43,44]. About 20,000 autopicked particles were used to generate the templates for all the particle auto-picking and about 500,000 particles were auto-picked from 2,200 micrographs for further processing. After two rounds of reference-free 2D classification and 3D classification, 53,465 particles within the best two classes were grouped and used for final refinement and following post-processing to converge into a map with a reported resolution of 7.82 Å (corrected gold-standard FSC 0.143 criteria). Chimera[45] was used to visualize and evaluate of the 3D maps, and the local resolution map was calculated using ResMap[46]. We also performed further local refinement but did not yield better density maps. The data processing is clearly presented in Supplementary Fig. 1.

Model building

For the modelling of dimeric ATM core regions (residues1425-3054), the previous model (PDB ID:5NP0)[17] was used as reference for building models. COOT[47] was used to manually fit the chains

into the density. The model of core region was finally refined with phenix.real_space_refine[48] against the 4.03 Å refined map.

The model of ATM core regions was docked into our EM map at 4.27 Å resolution using UCSF Chimera[45],and the previous model (PDB ID:5NP0)[17] was used as reference for building models to build the remaining part of ATM N-terminal. The overall model was finally refined with phenix.real_space_refine[48] against the 4.27 Å refined map.

As for the monomeric ATM, half of the model of dimeric ATM was docked into the 7.82 Å monomeric map, then manually fit the chains into the density, and finally refined with phenix.real_space_refine[48] against the map. The final statistics are listed in the Supplementary Table 1.

References:

1 Bhatti, S. *et al.* ATM protein kinase: the linchpin of cellular defenses to stress. *Cell Mol Life Sci* **68**, 2977-3006, doi:10.1007/s00018-011-0683-9 (2011).

2 Jackson, S. P. & Bartek, J. The DNA-damage response in human biology and disease. *Nature* **461**, 1071-1078, doi:10.1038/nature08467 (2009).

3 Lavin, M. F. Ataxia-telangiectasia: from a rare disorder to a paradigm for cell signalling and cancer. *Nat Rev Mol Cell Biol* **9**, 759-769, doi:10.1038/nrm2514 (2008).

4 McKinnon, P. J. ATM and the molecular pathogenesis of ataxia telangiectasia. *Annu Rev Pathol* **7**, 303-321, doi:10.1146/annurev-pathol-011811-132509 (2012).

5 Lovejoy, C. A. & Cortez, D. Common mechanisms of PIKK regulation. *DNA Repair (Amst)* **8**, 1004-1008, doi:10.1016/j.dnarep.2009.04.006 (2009).

6 Rivera-Calzada, A. *et al.* Structure and Assembly of the PI3K-like Protein Kinases (PIKKs) Revealed by Electron Microscopy. *Aims Biophysics* **2**, 36-57, doi:10.3934/biophy.2015.2.36 (2015).

7 Shiloh, Y. & Ziv, Y. The ATM protein kinase: regulating the cellular response to genotoxic stress, and more. *Nat Rev Mol Cell Biol* **14**, 197-210 (2013).

8 Paull, T. T. Mechanisms of ATM Activation. *Annu Rev Biochem* **84**, 711-738, doi:10.1146/annurev-biochem-060614-034335 (2015).

9 Stracker, T. H., Roig, I., Knobel, P. A. & Marjanovic, M. The ATM signaling network in development and disease. *Front Genet* **4**, 37, doi:10.3389/fgene.2013.00037 (2013).

10 Canman, C. E. *et al.* Activation of the ATM kinase by ionizing radiation and phosphorylation of p53. *Science* **281**, 1677-1679 (1998).

11 Bakkenist, C. J. & Kastan, M. B. DNA damage activates ATM through intermolecular autophosphorylation and dimer dissociation. *Nature* **421**, 499-506, doi:10.1038/nature01368 (2003).

12 Lee, J. H. & Paull, T. T. Direct activation of the ATM protein kinase by the Mre11/Rad50/Nbs1 complex. *Science* **304**, 93-96, doi:10.1126/science.1091496 (2004).

13 Hartlerode, A. J., Morgan, M. J., Wu, Y., Buis, J. & Ferguson, D. O. Recruitment and activation of the ATM kinase in the absence of DNA-damage sensors. *Nat Struct Mol Biol* **22**, 736-743, doi:10.1038/nsmb.3072 (2015).

14 Lee, J. H. & Paull, T. T. ATM activation by DNA double-strand breaks through the Mre11-Rad50-Nbs1 complex. *Science* **308**, 551-554, doi:10.1126/science.1108297 (2005).

15 Dupre, A., Boyer-Chatenet, L. & Gautier, J. Two-step activation of ATM by DNA and the Mre11-Rad50-Nbs1 complex. *Nat Struct Mol Biol* **13**, 451-457, doi:10.1038/nsmb1090 (2006).

16 Wang, X. *et al.* Structure of the intact ATM/Tel1 kinase. *Nat Commun* **7**, 11655, doi:10.1038/ncomms11655 (2016).

17 Baretic, D. *et al.* Structures of closed and open conformations of dimeric human ATM. *Sci Adv* **3**, e1700933, doi:10.1126/sciadv.1700933 (2017).

18 Lau, W. C. *et al.* Structure of the human dimeric ATM kinase. *Cell Cycle* **15**, 1117-1124, doi:10.1080/15384101.2016.1158362 (2016).

19 Llorca, O., Rivera-Calzada, A., Grantham, J. & Willison, K. R. Electron microscopy and 3D reconstructions reveal that human ATM kinase uses an arm-like domain to clamp around double-stranded DNA. *Oncogene* **22**, 3867-3874, doi:10.1038/sj.onc.1206649 (2003).

20 Brown, A. L. *et al.* A human Cds1-related kinase that functions downstream of ATM protein in the cellular response to DNA damage. *Proc Natl Acad Sci U S A* **96**, 3745-3750 (1999).

21 Guo, Z., Kozlov, S., Lavin, M. F., Person, M. D. & Paull, T. T. ATM activation by oxidative stress. *Science* **330**, 517-521, doi:10.1126/science.1192912 (2010).

22 Yang, H. *et al.* mTOR kinase structure, mechanism and regulation. *Nature* **497**, 217-223, doi:10.1038/nature12122 (2013).

23 Rao, Q. *et al.* Cryo-EM structure of human ATR-ATRIP complex. *Cell Res* **28**, 143-156, doi:10.1038/cr.2017.158 (2018).

24 Yin, X., Liu, M., Tian, Y., Wang, J. & Xu, Y. Cryo-EM structure of human DNA-PK holoenzyme. *Cell Res* **27**, 1341-1350, doi:10.1038/cr.2017.110 (2017).

25 Yang, H. *et al.* Mechanisms of mTORC1 activation by RHEB and inhibition by PRAS40. *Nature* **552**, 368-373, doi:10.1038/nature25023 (2017).

26 Yang, H. *et al.* 4.4 A Resolution Cryo-EM structure of human mTOR Complex 1. *Protein Cell* **7**, 878-887, doi:10.1007/s13238-016-0346-6 (2016).

27 Chen, X. *et al.* Cryo-EM structure of human mTOR complex 2. *Cell Res* **28**, 518-528, doi:10.1038/s41422-018-0029-3 (2018).

28 Wang, X. J. *et al.* 3.9 angstrom structure of the yeast Mec1-Ddc2 complex, a homolog of human ATR-ATRIP.

Science **358**, 1206-1209, doi:10.1126/science.aan8414 (2017).
29 Shiotani, B. & Zou, L. Single-Stranded DNA Orchestrates an ATM-to-ATR Switch at DNA Breaks. *Molecular Cell* **33**, 547-558, doi:10.1016/j.molcel.2009.01.024 (2009).
30 You, Z., Bailis, J. M., Johnson, S. A., Dilworth, S. M. & Hunter, T. Rapid activation of ATM on DNA flanking double-strand breaks. *Nat Cell Biol* **9**, 1311-1318, doi:10.1038/ncb1651 (2007).
31 Adamowicz, M. Breaking up with ATM. *J Immunol Sci* **2**, 26-31 (2018).
32 You, Z., Chahwan, C., Bailis, J., Hunter, T. & Russell, P. ATM activation and its recruitment to damaged DNA require binding to the C terminus of Nbs1. *Mol Cell Biol* **25**, 5363-5379, doi:10.1128/MCB.25.13.5363-5379.2005 (2005).
33 Kanu, N. & Behrens, A. ATMIN defines an NBS1-independent pathway of ATM signalling. *EMBO J* **26**, 2933-2941, doi:10.1038/sj.emboj.7601733 (2007).
34 Mordes, D. A., Glick, G. G., Zhao, R. & Cortez, D. TopBP1 activates ATR through ATRIP and a PIKK regulatory domain. *Genes Dev* **22**, 1478-1489, doi:10.1101/gad.1666208 (2008).
35 Adamowicz, M., Vermezovic, J. & d'Adda di Fagagna, F. NOTCH1 Inhibits Activation of ATM by Impairing the Formation of an ATM-FOXO3a-KAT5/Tip60 Complex. *Cell Rep* **16**, 2068-2076, doi:10.1016/j.celrep.2016.07.038 (2016).
36 Vermezovic, J. *et al.* Notch is a direct negative regulator of the DNA-damage response. *Nature Structural & Molecular Biology* **22**, 417-424, doi:10.1038/nsmb.3013 (2015).
37 Lee, J. H. *et al.* ATM directs DNA damage responses and proteostasis via genetically separable pathways. *Sci Signal* **11**, doi:10.1126/scisignal.aan5598 (2018).
38 Lee, J. H., Guo, Z., Myler, L. R., Zheng, S. & Paull, T. T. Direct activation of ATM by resveratrol under oxidizing conditions. *PLoS One* **9**, e97969, doi:10.1371/journal.pone.0097969 (2014).
39 Clare, D. K. *et al.* Electron Bio-Imaging Centre (eBIC): the UK national research facility for biological electron microscopy. *Acta Crystallogr D Struct Biol* **73**, 488-495, doi:10.1107/S2059798317007756 (2017).
40 Campbell, M. G. *et al.* Movies of ice-embedded particles enhance resolution in electron cryo-microscopy. *Structure* **20**, 1823-1828, doi:10.1016/j.str.2012.08.026 (2012).
41 de la Rosa-Trevin, J. M. *et al.* Scipion: A software framework toward integration, reproducibility and validation in 3D electron microscopy. *J Struct Biol* **195**, 93-99, doi:10.1016/j.jsb.2016.04.010 (2016).
42 Zheng, S. Q. *et al.* MotionCor2: anisotropic correction of beam-induced motion for improved cryo-electron microscopy. *Nat Methods* **14**, 331-332, doi:10.1038/nmeth.4193 (2017).
43 Zhang, K. Gctf: Real-time CTF determination and correction. *J Struct Biol* **193**, 1-12, doi:10.1016/j.jsb.2015.11.003 (2016).
44 Zivanov, J. *et al.* RELION-3: new tools for automated high-resolution cryo-EM structure determination. *bioRxiv*, doi:10.1101/421123 (2018).
45 Pettersen, E. F. *et al.* UCSF Chimera--a visualization system for exploratory research and analysis. *J Comput Chem* **25**, 1605-1612, doi:10.1002/jcc.20084 (2004).
46 Kucukelbir, A., Sigworth, F. J. & Tagare, H. D. Quantifying the local resolution of cryo-EM density maps. *Nat Methods* **11**, 63-65, doi:10.1038/nmeth.2727 (2014).
47 Emsley, P., Lohkamp, B., Scott, W. & Cowtan, K. Features and development of Coot. *Acta Crystallographica Section D: Biological Crystallography* **66**, 486-501 (2010).
48 Adams, P. D. *et al.* PHENIX: a comprehensive Python-based system for macromolecular structure solution. *Acta Crystallographica Section D: Biological Crystallography* **66**, 213-221 (2010).

Acknowledgments

We thank Center for Biological Imaging (CBI) of Institute of Biophysics (IBP) of Chinese Academy of Sciences (CAS) and National Center for Protein Science Shanghai (NCPSS) for the support on cryo-EM data collection and data analyses. We thank staff members Biomedical Core Facility, Fudan University for their help on Mass Spectrometry analyses. This work was supported by grants from the Ministry of Science and Technology of China (2016YFA0500700), the National Natural Science Foundation of China (U1432242, 31425008), the National Program for support of Top-Notch Young Professionals (Y. X.), the Strategic Priority Research Program of the Chinese Academy of Sciences (grant no. XDB08000000), and the UK Wellcome Trust Investigator Award 206422/Z/17/Z (P. Z.). We acknowledge Diamond for access of the Cryo-EM facilities at the UK national electron bio-imaging centre (eBIC, proposal NT21004), funded by the Wellcome Trust, MRC and BBSRC.

Author contributions

J. X., M. L., Y. Q, and Y. X. designed the experiments. J. X., Y. Q., and C. G. purified the proteins. M. L., Y. C., P. Z., Y. Q., Y. T., and Z. Y. prepared the cryo-EM sample, collected the data and determined the structures. M. L. built the structural model. J. X., B. P, and Y. X. performed biochemical analyses. J. X., M. L., and Y. X. analyzed the data and wrote the manuscript with support from all the authors. Y. X. supervised the project.

Data and materials availability:

The electron density map and corresponding atomic coordinates will be deposited during revision.

The authors declare no competing financial interests.

Figures and Figure legends

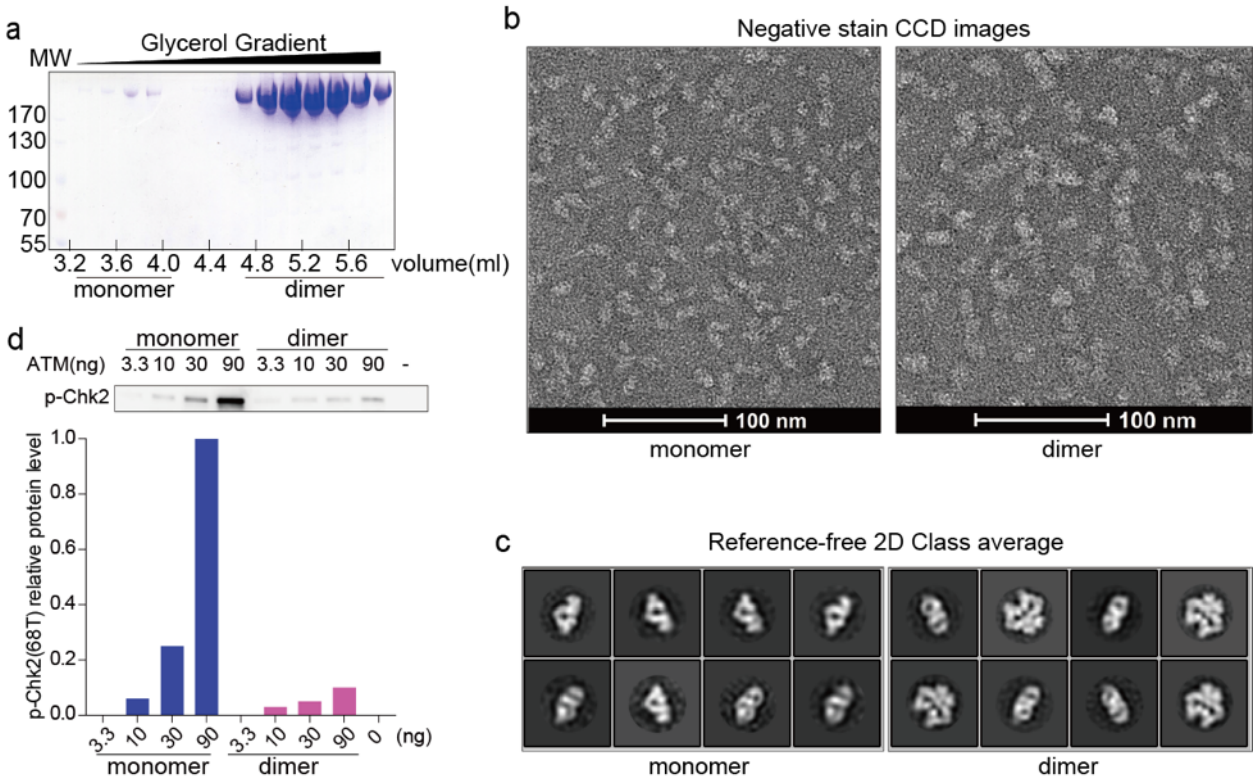


Fig. 1. Purification and characterization of monomeric and dimeric ATM

(a). Separation of monomeric and dimeric ATM using glycerol gradient centrifugation. The fractions were subjected to SDS-PAGE and stained using Coomassie blue. The fraction volumes were indicated below the figure.

(b). Representative micrographs of negative staining EM image of dimeric and monomeric ATM. The peak fractions as shown in Fig. 1a. were used for grids preparation.

(c). Reference-free 2D class averages of monomeric and dimeric ATM. Particles were picked from the images of Fig. 1b. The majority of the particles are in monomeric (left) and dimeric (right) form, respectively. Note that ATM dimer has two representative views, the front view (butterfly shape, such as bottom left) and bottom view (double ring shape, such as top left).

(d). *In vitro* kinase assay using increasing amount of purified monomeric and dimeric ATM kinases. The purified human Chk2 (1 μg) serves as substrate. The reaction was subjected to SDS-

PAGE and visualized by immunoblotting (8 μl reaction products) with antibody specifically targeting phospho-Thr-68 of Chk2. Bar representations of the relative kinase activities were generated according to the immunoblotting results.

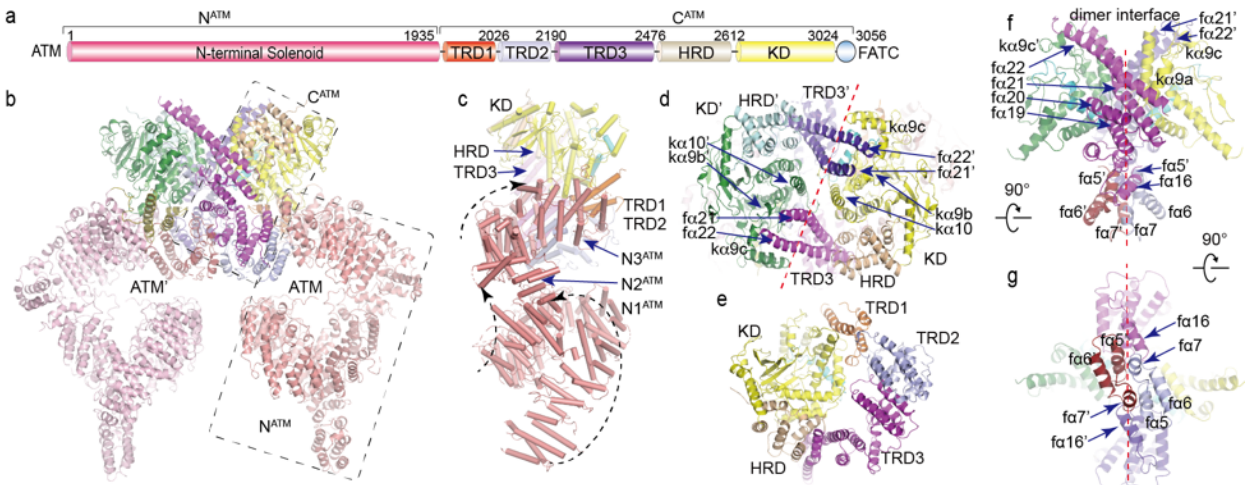


Fig. 2. Overall structure of dimeric ATM

(a). Color-coded domain structure of human ATM with boundaries indicated with numbers above the schematic representation. The same color scheme is used in all structure figures for one ATM (right one in Fig. 1b) in dimer if not specified elsewhere. The FAT domain consists of TRD1-TRD3 and HRD. We refer the FAT, KD, and FATC to as the C^{ATM} and the N-terminal solenoid as N^{ATM} for simplicity.

(b-d). Ribbon representations of dimeric ATM in front view (b), side view (c), and top view (d), respectively. The ATM molecule in right side is colored as in Fig. 2a. The molecule in left side is colored in salmon (N^{ATM}), olive (TRD1), red (TRD2), blue (TRD3), cyan (HRD), green (KD), and lightbule (FATC), respectively. In Fig. 2c, side-view of one monomer in ATM dimer with the helices shown in cylinders. The path of N-terminal solenoid, from N- to C-terminus, is indicated with arrows.

(e). Close-up view of the kinase domain that is wrapped by the FAT domain.

(f-g). Dimer interface shown in two different views. The critical helices for dimerization are indicated.

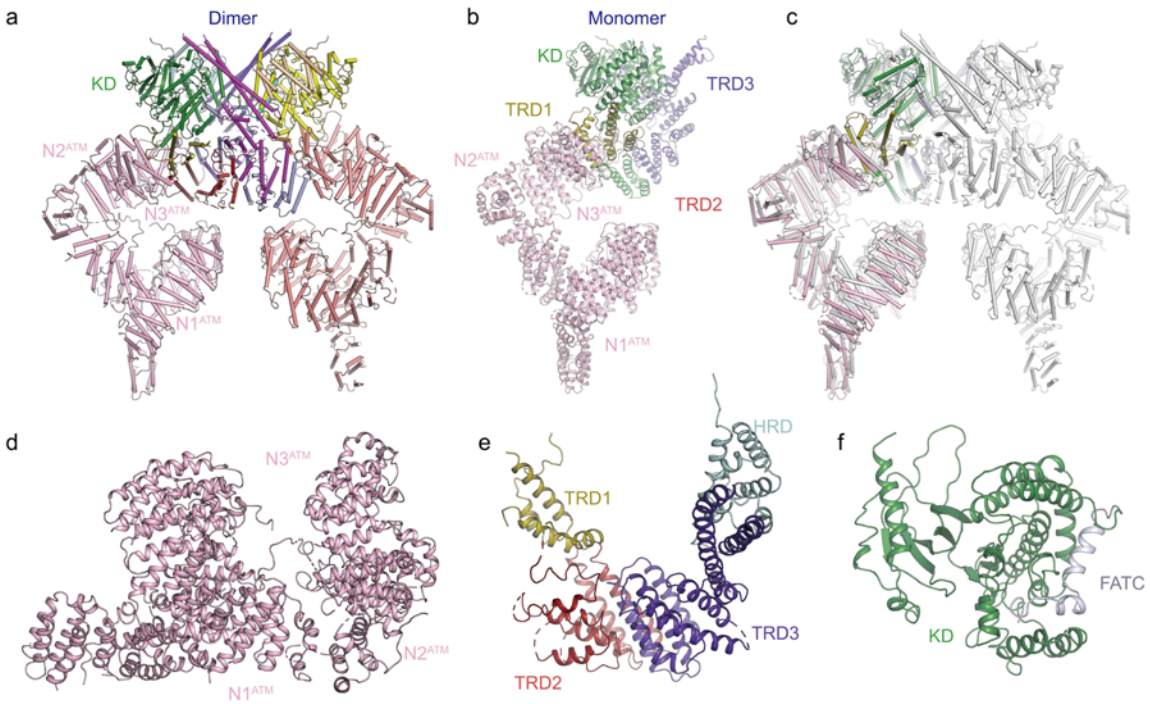


Fig. 3. Structures of ATM monomer and dimer

(a-c). Structures of ATM dimer (a), monomer (b), and superimposition of dimer and monomer (c). The structures are shown in an orientation as in Fig. 2b.

(d-f) Close-up views of isolated domains of ATM. The ATM dimer model was used for the analysis.

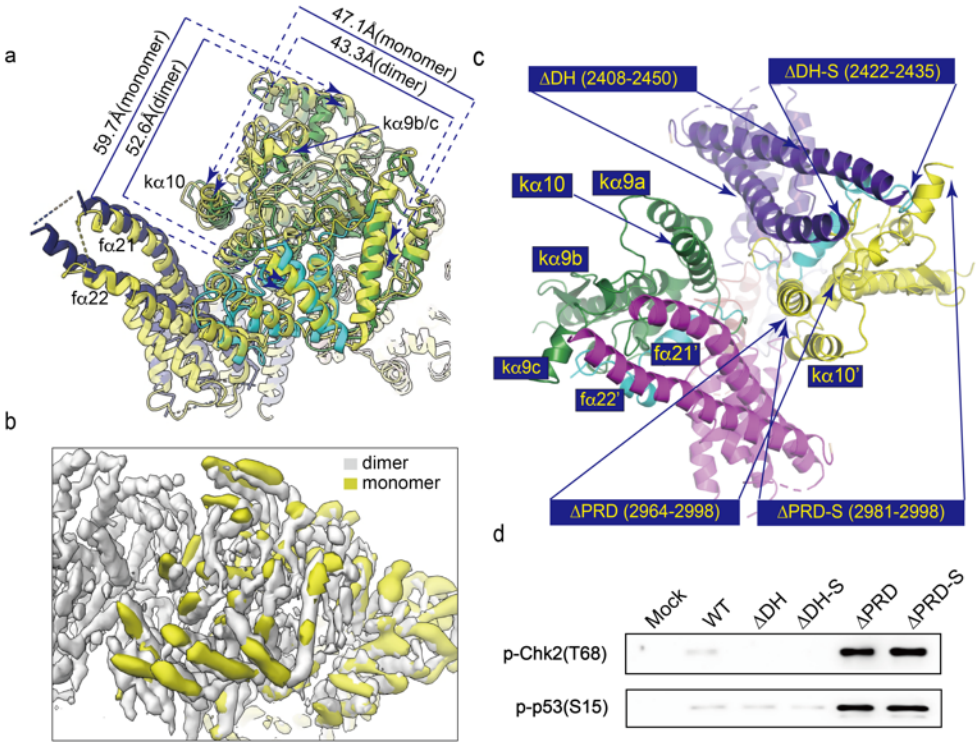


Fig. 4 ATM monomer structure and comparison with dimer

(a-b). Structural comparison of ATM dimer and monomer. Ribbon representations (a) and cryo-EM maps (b) of ATM dimer and monomer are shown in a similar view. One ATM monomer in the dimer is omitted in Figure (a) for clarity. The ATM dimer is colored in yellow. The heights (distance between Cα atoms of residue D2597 and D2795) and widths (distance between Cα atoms of residue M3011 and A2626) of the catalytic pockets of ATM dimer and monomer are indicated for comparison.

(c). A top view structure of ATM dimer showing critical regulatory elements for dimerization and kinase activity. The regions that are deleted in the four ATM mutants are indicted with arrows.

(d). *In vitro* kinase assay using purified wild type ATM and four ATM mutants in equal concentration (20 ng). The assays were performed as in Fig. 1d. The purified human Chk2 (1 μg)

and p53 (0.7 μg) were used as substrates, respectively. The activities were visualized with antibodies against phospho-Thr-68 of Chk2 and phospho-Ser-15 of p53, respectively.

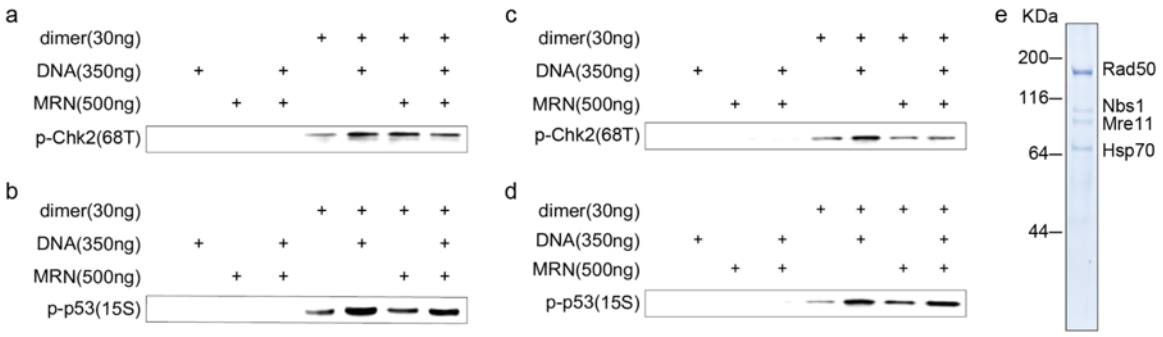
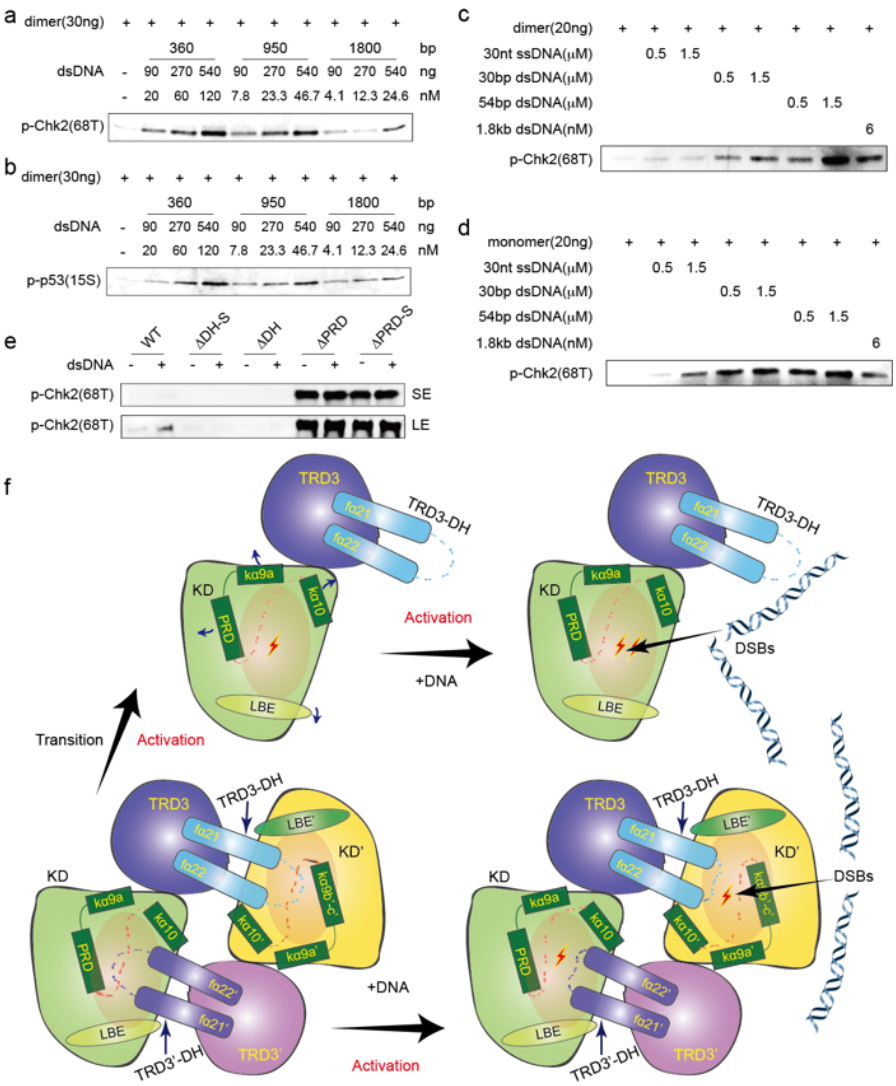


Fig. 5. MRN-mediated ATM activation

(a-c). Kinase assays were performed with recombinant 30ng dimeric ATM, 500ng MRN and 350ng 950bp dsDNA, 1μg purified human catalytic mutant Chk2 (a, c) and p53 (b, d) serves as substrates, respectively. The reactions were performed in 20μl with KCl concentration of 50mM (a, b) or 200mM (c, d), respectively. The reaction products (8μl) were subjected to SDS-PAGE and the activities were detected by immunoblotting with antibody specifically targeting phospho-Thr-68 of Chk2 (a, c) and phospho-Ser-15 of p53 (b, d).

(e). The purified MRN complex used for the kinase assay were subjected to SDS-PAGE and stained using Coomassie blue.



627

628 **Fig. 5. DNA-mediated activation of ATM and a model for ATM activation**

629 (a-b). The *in vitro* kinase assays were performed using dimeric ATM (30ng) in the presence of
630 increasing amount of DNA fragments in three different lengths. The lengths and amounts of
631 DNA were indicated. 1μg purified human Chk2 (a) and 0.7μg p53 (b)serves as substrate in 20μl
632 50mM KCl system. The reactions were subjected to SDS-PAGE for immunoblotting with the
633 activities detected by antibodies against phospho-Thr-68 of Chk2 (a) and phospho-Ser-15 of p53
634 (b).

635 (c-d). Short DNA could activate ATM dimer (c) and monomer (d). The kinase assays were
636 performed as in Fig. 5a with the lengths and amounts of DNA indicated.

(e). The *in vitro* kinase assays were performed using equal amount (20 ng) of purified wild-type ATM and ATM mutants in the absence or presence of 1.8kb dsDNA (500 ng).

(f). A working model that illustrates the mechanism for ATM activation in response to DNA damage (see main text).